Orbital
The electronic journal of chemistry

the electronic journal of chemistry

Full paper | http://dx.doi.org/10.17807/orbital.v13i2.1453

Simulation of the Impedance of the Electrical Double Layer and Evaluation of the Surface Excess Concentration by Finite Element Analysis

Alex Silva de Moraes [a*], Evaldo Batista Carneiro Neto [b], and Mauro Chierici Lopes [a]

Understanding the structure of the electrical double layer (EDL) is of great importance for many different technological and scientific applications, but some information is not always accessible from experiments. In this sense, the aim of this study was to implement a simple one-dimensional computational model for the study of the EDL and solve by the finite element method. The details of the validation of the model are presented and frequency domain analysis is performed in order to obtain impedance information. From the impedance study, it was possible to obtain the total capacitance and confirm its dependence on applied potential. Moreover, calculations of the Gibbs excess surface concentration were carried out for different values of bulk concentration. Our results are in agreement with analytical predictions, showing that the model is suitable for the study of the EDL structure.

Graphical abstract

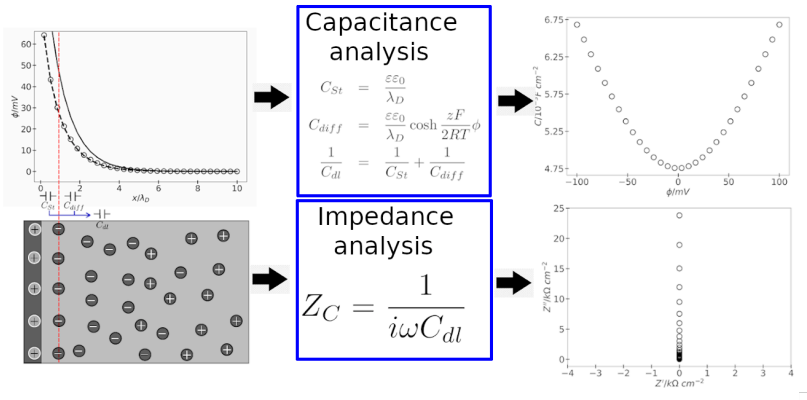

Keywords

Computational electrochemistry
Double layer capacitance
Electrical double layer
Finite element analysis
Impedance spectroscopy

Article history

Received 28 November 2019
Revised 25 January 2021
Accepted 25 January 2021
Available online 03 February 2021

Handling Editor: Sergio R. Lázaro

1. Introduction

In the absence of irreversible processes, particles in a bulk electrolyte experience isotropic forces, so that there is no net force acting upon them and therefore no alignment of their dipole momentum in any specific direction. However, the presence of another phase, such as the electrode, creates an anisotropic distribution of forces near the surface, changing the structure of this interphasial region, creating a new structure known as electrical double layer (EDL) [1].

The first model to describe the EDL structure is Helmholtz model [1, 2]. In this model, ions in solution are assumed to be distributed over a two-dimensional layer with charge *q*, while the electrode has a charge *-q*. The double layer structure is then treated as a parallel plate capacitor. A few decades later,

[a] Department of Chemistry, Universidade Estadual do Centro–Oeste, Guarapuava, PR, 85040-167, Brazil. [b] LIEC - DQ- Universidade Federal de São Carlos, São Carlos, SP, 13565-905, Brazil. *Corresponding author. E-mail: **asmoraes92@gmail.com**

Gouy and Chapman developed another model, known as Gouy-Chapman model [1, 2]. In this model, the ions are treated as point charges and are distributed through the solution in a region called diffuse layer. The ion distribution is assumed to follow Boltzmann distribution and the potential is solved through Poisson equation and the combined solution is called Poisson-Boltzmann equation [2]. However, at steady state this equation is equivalent to the Poisson-Nernst-Planck (PNP) equation, as will be shown in section 1.1, which is obtained by combining Poisson equation for the electric potential and the Nernst-Planck equation for ion transport in solution.

Another model for the EDL structure came later and is known as Stern model, which is a combination of Helmholtz and Gouy-Chapman models [1, 2]. The structure of the EDL as described by Stern is shown in Figure 1, where Ch and Cd are the Helmholtz and diffuse capacitances, calculated from Helmholtz and Gouy-Chapman models, respectively; Ct is the total capacitance, obtained by the series combination of Ch and Cd. The lower part of the figure shows the potential drop in the electrolyte phase due to the ion distribution in the EDL.

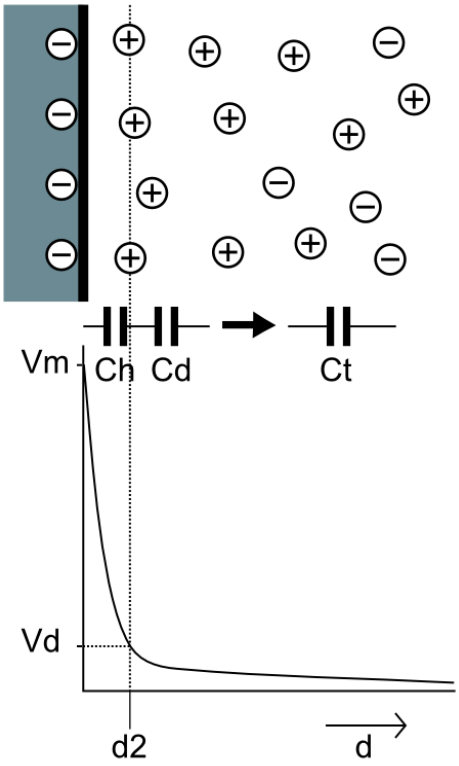

Fig. 1. Electrical double layer structure [3].

In laboratory experiments it is usual to add sufficient quantity of supporting electrolyte to confine the EDL to a thin layer much smaller than the diffusion layer and then ignore its structure. There are practical situations, however, where the double layer structure plays a major role such as in EDL supercapacitors [4-6] and in interfaces between two immiscible electrolyte solutions (ITIES) [7-11]. The study and design of these devices rely on a suitable model of the double layer structure and the resultant electrical properties. In this paper we present a simple model and its computational simulation using finite element analysis. The model is restricted to a one-dimensional domain and dilute solution approximation to keep the analytical solutions valid and allow the model validation. Furthermore, a frequency domain analysis is implemented in order to simulate impedance measurements, which are important to compare with experimental results. This model paves the way to more sophisticated approaches including geometric complications, such as porosity, and thermodynamic non-idealities, which happen in concentrated solutions. A few previous studies have been reported but without model validation and impedance calculations [12, 13].

1.1 Derivation of the PNP equation:

The Nernst-Planck equation (without the convection term) is given by:

$$\boldsymbol{J_i} = D_i \frac{\mathrm{dc_i}}{\mathrm{dx}} + z_i F c_i u_i \frac{\mathrm{d}\phi}{\mathrm{dx}} \tag{1}$$

where $\boldsymbol{J_i}$ is the flux of species i, D_i is the diffusion coefficient, c_i the concentration, $z_i F$ the charge, u_i the mobility and ϕ the electric potential.

Assuming stationary state, $\boldsymbol{J_i} = 0$, so equation (1) becomes [14]:

$$D_i \frac{\mathrm{dc_i}}{\mathrm{dx}} + z_i F c_i u_i \frac{\mathrm{d}\phi}{\mathrm{dx}} = 0 \tag{2}$$

Using the variable change

$$c_i = q_1 q_2 \tag{3}$$

where q_1 and q_2 are arbitrary functions of space coordinates (x in this case), equation (2) becomes:

$$D_i q_2 \frac{\mathrm{dq_1}}{\mathrm{dx}} + q_1 \left(D_i \frac{\mathrm{dq_2}}{\mathrm{dx}} + z_i F q_2 u_i \frac{\mathrm{d}\phi}{\mathrm{dx}} \right) = 0 \tag{4}$$

Since the choice of the functions q_1 and q_2 are arbitrary, it is possible to choose a q_2 that satisfies:

$$D_i \frac{\mathrm{dq_2}}{\mathrm{dx}} + z_i F q_2 u_i \frac{\mathrm{d}\phi}{\mathrm{dx}} = 0$$

which gives

$$q_2 = exp\left(\frac{z_i F}{RT}\phi\right) \tag{5}$$

where the Nernst-Einstein relation ($u_i = D_i/RT$) was used. Substituting this q_2 in equation (4), we obtain:

$$D_i exp\left(\frac{z_i F}{RT}\phi\right) \frac{\mathrm{dq_1}}{\mathrm{dx}} = 0 \tag{6}$$

For equation (6) to be valid, q_1 must be a constant. Furthermore, when $x \to \infty$, $\phi \to 0$ and $c_i \to c_i^*$, where c_i^* is the bulk concentration of species i. With this boundary condition and equations (3) and (5), we obtain:

$$c_i = c_i^* exp\left(-\frac{z_i F}{RT}\phi\right) \tag{7}$$

Poisson equation is given by:

$$\frac{d^2\phi}{dx^2} = -\frac{\rho(x)}{\varepsilon\varepsilon_0} \tag{8}$$

Where ε_0 is the vacuum permittivity, ε is the dielectric constant of the medium and $\rho(x)$ is the space charge density in the electrolyte, given by

$$\rho(x) = F[z_+ c_+(x) + z_- c_-(x)] \tag{9}$$

Substituting equations (7) and (9) into equation (8) and assuming $z_+ = z$ and $z_- = -z$, we obtain:

$$\frac{d^2\phi}{dx^2} = -\frac{zFc_0}{\varepsilon\varepsilon_0}\left[exp\left(-\frac{zF}{RT}\phi\right) - exp\left(\frac{zF}{RT}\phi\right)\right] \tag{10}$$

or

$$\frac{d^2\phi}{dx^2} = -\frac{2zFc_0}{\varepsilon\varepsilon_0}\sinh\left(\frac{zF}{RT}\phi\right) \quad (11)$$

which is the nonlinear PNP equation.

For potentials much smaller than the thermal voltage ($\phi \ll RT/F$), equation (10) becomes:

$$\frac{d^2\phi}{dx^2} = \frac{2(zF)^2c_0}{\varepsilon\varepsilon_0 RT}\phi(x) = \frac{1}{\lambda_D^2}\phi(x) \quad (12)$$

where λ_D is the Debye length, defined as

$$\lambda_D = \left(\frac{\varepsilon\varepsilon_0 RT}{2z^2F^2c_0}\right)^{\frac{1}{2}} \quad (13)$$

Equation (12) has the general solution

$$\phi(x) = Aexp\left(-\frac{x}{\lambda_D}\right) + Bexp\left(\frac{x}{\lambda_D}\right) \quad (14)$$

But since $\phi(x) \to 0$ when $x \to \infty$, we have $B = 0$. Constant A is given by the charge balance relation between the charge density on the metal side of the double layer (σ) and on the solution side ($\rho(x)$):

$$\sigma = -\int_0^\infty \rho(x)dx \quad (15)$$

We then obtain:

$$\phi(x) = \frac{\sigma\lambda_D}{\varepsilon\varepsilon_0}\, exp\left(-\frac{x}{\lambda_D}\right) \quad (16)$$

and the surface charge density is then

$$\sigma = \frac{\varepsilon\varepsilon_0}{\lambda_D} exp\left(\frac{x}{\lambda_D}\right)\phi(x) \quad (17)$$

The double layer capacitance is then given by

$$C = \left(\frac{d\sigma}{d\phi}\right)_{x=0} = \frac{\varepsilon\varepsilon_0}{\lambda_D} \quad (18)$$

Equations (16), (17) and (18) correspond to the linear approximation of the PNP equation. If one solves the nonlinear PNP equation, the results for the potential, surface charge density and capacitance are as follows:

$$\phi(x) = \frac{4RT}{zF}\tanh^{-1}\left[\frac{\sqrt{1+\alpha^2\sigma^2}-1}{\alpha\sigma}exp\left(-\frac{x}{\lambda_D}\right)\right] \quad (19)$$

$$\sigma = \frac{1}{\alpha}\sinh\left[\frac{zF}{2RT}\phi(0)\right] \quad (20)$$

where $\alpha = (8RTc_0\varepsilon\varepsilon_0)^{1/2}$, and

$$C = \frac{\varepsilon\varepsilon_0}{\lambda_D}\cosh\left(\frac{zF}{2RT}\phi\right) \quad (21)$$

For the derivation of the nonlinear solution the reader is redirected to specialized references [1, 2].

1.2 Excess surface concentration

Before the immersion of the electrode into the solution, the concentration of species i is everywhere the same and it equals the bulk concentration c_i^*. But after the electrode is immersed and the double layer is formed, the steady state concentration distribution is no longer the same at every point. Suppose the electrode charges negatively. There will be an accumulation of cations and a depletion of anions in the interphase and the concentration c_i of the ions can be higher (for accumulation) or lower (for depletion) than the bulk concentration. However, changes in concentration are often preferred rather than their actual values [1]. Therefore, we define the change in concentration $c_i'(x)$ as

$$c_i'(x) = c_i(x) - c_i^* \quad (22)$$

We can now define the Gibbs excess surface concentration of species i (Γ_i) as the total concentration stored at the double layer in respect to the bulk concentration [1]:

$$\Gamma_i = \int_0^\infty c_i'(x)dx = \int_0^\infty [c_i(x) - c_i^*]dx \quad (23)$$

The concept of surface excess is very important, because it is related to quantities such as interfacial tension and its dependence on concentration [1]. Furthermore, direct measurements of excess surface are achievable experimentally [1, 15].

1.3 Frequency domain analysis

For the frequency domain analysis, a harmonic potential perturbation was applied to the electrode surface according to

$$\phi_M = \phi_{dc} + \phi_0\sin(\omega t) \quad (24)$$

where ϕ_M is the potential at the electrode surface, ϕ_{dc} is the dc voltage applied by an external source, ϕ_0 is the amplitude of the perturbation and ω is the angular frequency.

For the current analysis, since there is no faradaic reaction, only a capacitive charging/discharging current exists and is given by the displacement current (25)

$$j_d = \varepsilon\varepsilon_0\left(\frac{\partial E}{\partial t}\right) = -\varepsilon\varepsilon_0\frac{\partial}{\partial t}\left(\frac{\partial\phi}{\partial x}\right) \quad (25)$$

In order to work in the frequency domain, it is necessary to apply the Laplace transform on equation (25), which becomes

$$j_d = -i\omega\varepsilon\varepsilon_0\left(\frac{\partial\phi}{\partial x}\right) \quad (26)$$

where i is the imaginary number.

For the potential, the Laplace transform is not necessary because the software used has a built-in operator that can be used in this case. This will be discussed in section 2.

The impedance Z is then defined as

$$Z = \frac{\phi_0\sin(\omega t)}{-i\omega\varepsilon\varepsilon_0\left(\frac{\partial\phi}{\partial x}\right)} \quad (27)$$

For a capacitor, the impedance Z_C is given by

$$Z_C = \frac{1}{i\omega C_{dl}} \quad (28)$$

where C_{dl} is the double layer capacitance.

2. Material and Methods

The simulations in this study were carried out in the finite element software COMSOL Multiphysics® version 5.4 [16]. All simulations were run in a computer with 8GB DDR4 RAM, intel core i5 8265u processor and a 2GB dedicated video card NVIDIA MX110.

The model assumed a one-dimensional geometry with two nodes, one taken as the electrode surface and the other taken

as the bulk of the electrolyte. A binary 1:1 electrolyte with an oxidized and a reduced species was defined and dilute solution transport theory was assumed.

The mesh was defined with the total of 232 elements. For the electrode boundary node, the maximum element size was 9.6198×10^{-13}m and for the rest of the domain, it was 4.8099×10^{-11}m. The element growth rate was of 1.3, which means that each element is 30% larger than the previous element. This growth only happens near the surface boundary, since in the electrolyte domain all elements have the same size.

For the validation of the model, the numerical solution was compared with the analytical solution of the PNP equation for low potentials (linear solution) and high potentials (nonlinear solution). The results for the validation process are shown in Figures 1 and 2. The potential at the electrode was varied, for the linear solution, from -20mV to 20mV and for the nonlinear solution, from -100mV to 100mV.

For the electrochemical impedance spectroscopy study, an ac voltage of 5mV was applied over the stationary dc voltage, which was varied from -100mV to +100 mV. The frequencies used for the ac voltage varied from 10^{-1} to 10^{3} Hz.

For the application of the ac voltage, COMSOL has a built-in operator, called *linper* that applies a linear perturbation to a function where it takes the input as the amplitude of oscillation. This operator can be used only for input variables, such as the potential [17]. For the response variables, such as the current density, the explicit expression in the frequency domain (obtained by the Laplace transform, in section 1.3) has to be defined.

For the surface excess concentration calculations the potential was varied from -100mV to 100mV and the bulk concentration was varied from 10^{-2} to 1 mol.L^{-1}.

Figure 2 shows the potential distribution as a function of position x (in units of Debye length), where the circle refers to the numerical solution, the solid line refers to the nonlinear solution and the dashed line refers to the linear solution. In Figure 2a, the applied potential is 100mV, which is greater than the thermal voltage $RT/F \approx 25mV$. In this region, we can see that potential distribution cannot be described by equation (16), which is the linear approximation, and has to be described by equation (19). In Figure 2b, the applied potential is 20mV. Here, the linear and nonlinear solutions coincide and therefore, the dashed line cannot be seen. In this region, the linear solution is valid and equation (16) can be used for the potential distribution. In both figures, the numerical solution agrees perfectly with the nonlinear solution, which shows that the simulation is in agreement with theory.

Figure 3 shows the surface charge density (σ) as a function of applied potential. As in Figure 2, the circle refers to the numerical solution, the solid line refers to the nonlinear solution and the dashed line refers to the linear solution. In Figure 3a, the applied potential was varied from -100mV to +100mV. We can see that for potentials greater that the thermal voltage, the linear approximation fails, while the nonlinear solution agrees with the numerical results. Figure 3b is an enlargement of the region ranging from -20mV to +20mV of Figure 2a and shows that in this range of potentials, the linear approximation holds true.

These results show that our model is in agreement with the expected results from the theory. From the data presented in Figure 3 it is possible to derivate the curves and therefore obtain the differential Gouy-Chapman capacitance.

3. Results and Discussion

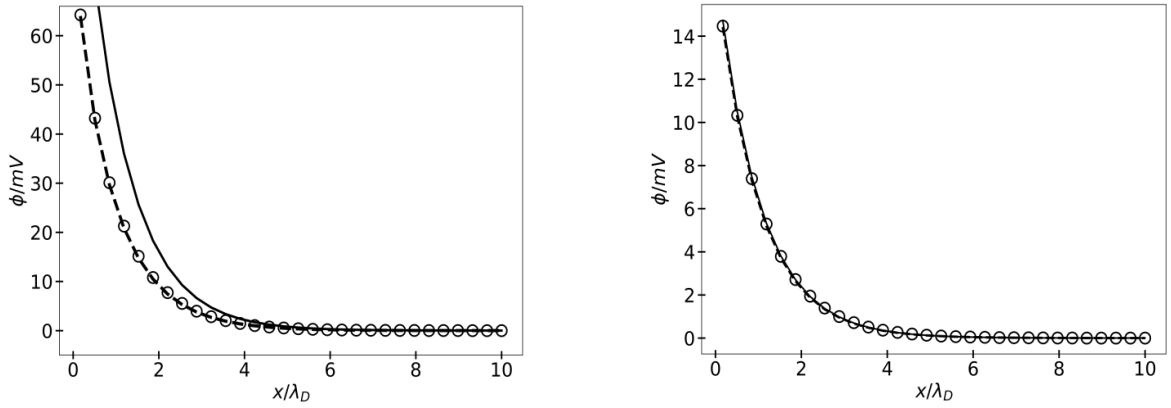

(a) 100mV **(b) 20mV**

Fig. 2. Potential distribution curves for the numerical (circles), linear (dashed lines) and nonlinear (solid lines) solutions.

Figure 4 shows the space charge density distribution (ρ_{space}) for +20mV and +100mV (lower dashed and solid lines, respectively), and for -20mV and -100mV (upper dashed and solid lines, respectively) as a function of position. We can see that, for positive potentials, there is an accumulation of negative charge on the solution side, and for negative potentials, the accumulation is of positive charges, as is expected from charge conservation condition.

Figure 5 shows the concentration profile for the cation and the anion for 100mV (5a) and 20mV (5b) divided by the bulk concentration c^*, which is shown by the dashed line. The lower curves refer to the cation concentration and the upper curves refer to the anion concentration. It is possible to notice in Figure 5 that when the potential is lower, the anion and the cation concentration profile are more symmetric with the bulk concentration than for higher potentials. The reason for this asymmetry is that the concentration cannot be less than zero and, therefore, as the potential increases, for example, in the negative direction, the interphasial region starts to lack anions to deplete, so, in order to compensate the electrode charge

and to achieve the space charge density profile shown in Figure 4, more cations need to be attracted, causing the asymmetry shown in Figure 5a for high potentials.

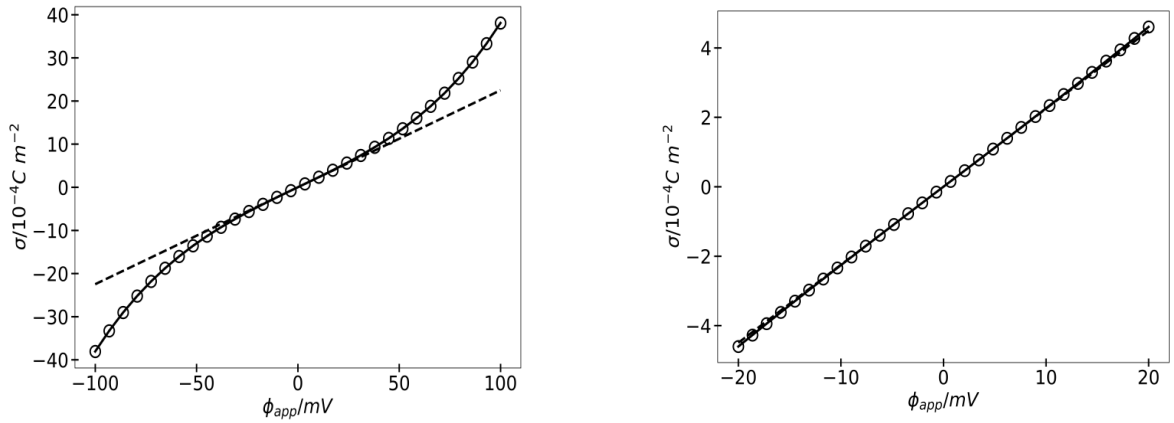

(a) high potentials **(b) low potentials**

Fig. 3. Surface charge distribution for numerical (circles), linear (dashed lines) and nonlinear (solid lines) solutions.

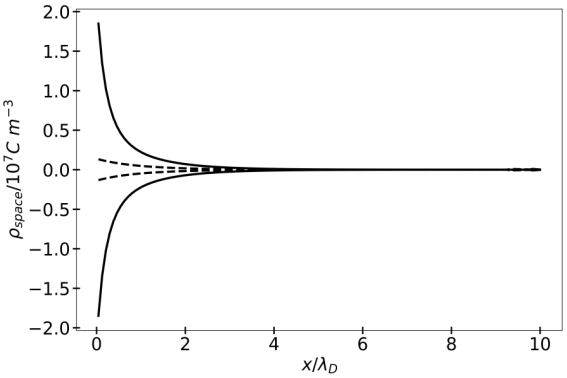

Fig. 4. Space charge density distribution for ±100mV (solid lines) and ±20mV (dashed lines).

Figure 6 shows the excess surface concentration for bulk concentrations of 0.01mol/L (solid line), 0.1mol/L (dotted line) and 1mol/L (dashed line) as a function of applied potential. Values of excess surface can be as high as $60x10^{-8}$ mol/m^2 and as low as $-30x10^{-8}$ mol/m^2, which shows the same asymmetry showed in Figure 3. Negative values of excess concentration mean depletion, while positive values mean attraction of ions.

Figure 7a shows the Nyquist diagram for applied dc potential of 100mV for frequencies varying from 10^{-1}Hz to 10^3Hz. *Z'* refers to real part of the impedance and *Z''* refers to its imaginary part. Since our simulation models a blocking electrode, no faradaic reactions occur and, therefore, the impedance spectrum is that of an ideal capacitor. Figure 7b shows the phase angle (θ) as a function of frequency (f) and, as expected for a capacitor, it is 90 degrees for all frequencies.

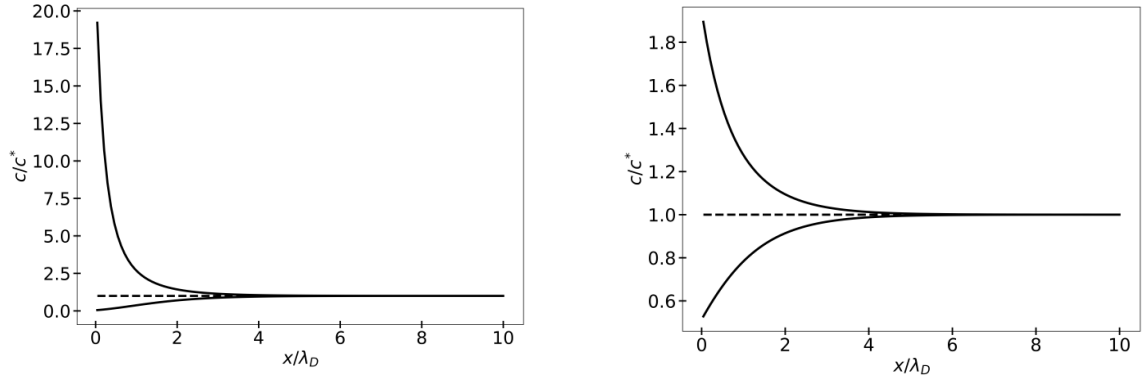

(a) 100mV **(b) 20mV**

Fig. 5. Concentration distribution cation (lower curves) and anion (upper curves). Dashed line refers to the bulk concentration.

Figure 8a shows the Nyquist diagram for frequency of 1Hz for five different dc potentials. Star is for 20mV, circle for 40mV, diamond for 60mV, square for 80mV and plus sign for 100mV. Since the capacitance is inversely proportional to the imaginary value of the impedance, we can see that as the potential increases, the imaginary impedance decreases and the capacitance increases, as shown in Figure 8b for the entire range of potentials.

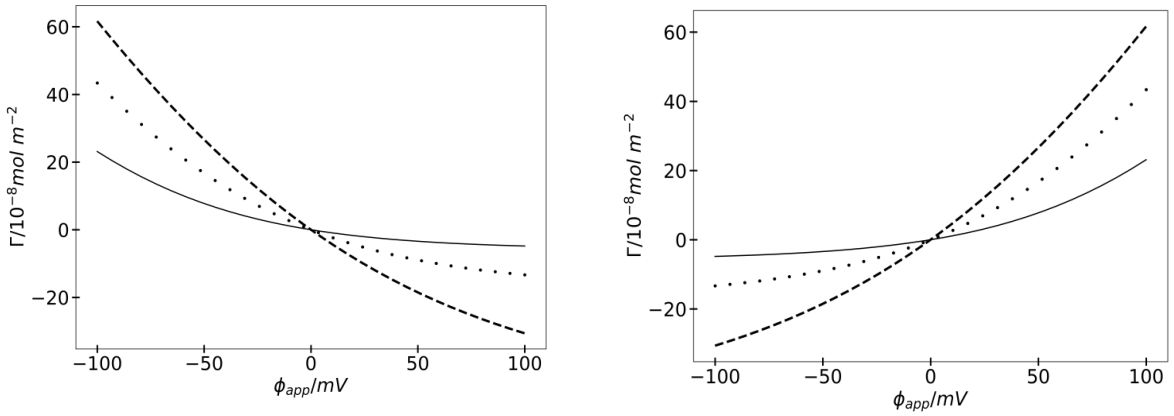

(a) Cation **(b) Anion**

Fig. 6. Excess surface concentration for 0.01mol/L (solid line), 0.1mol/L (dotted line) and 1mol/L (dashed line).

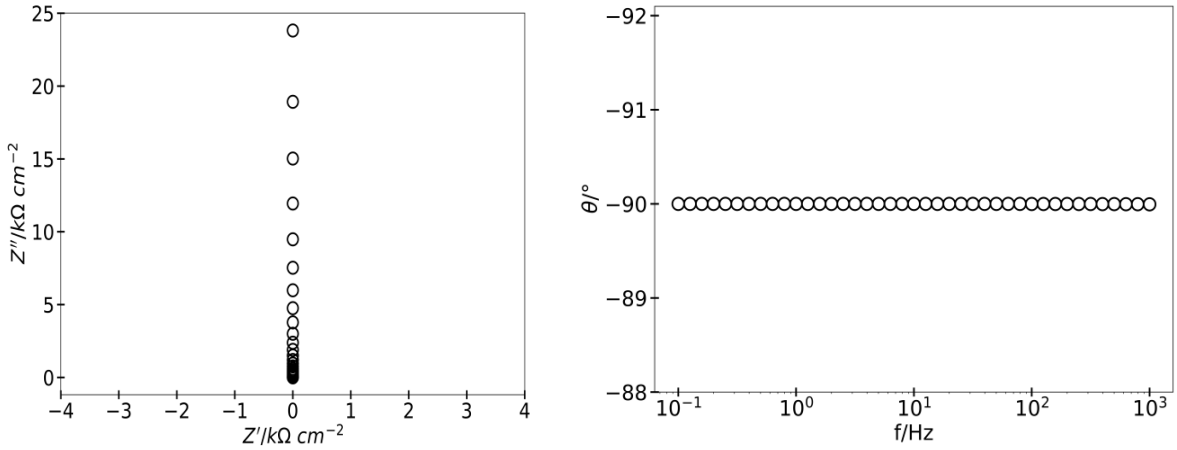

(a) Nyquist diagram **(b) Phase angle**

Fig. 7. Results of impedance study for frequencies varying from 10^{-1}Hz to 10^{3}Hz.

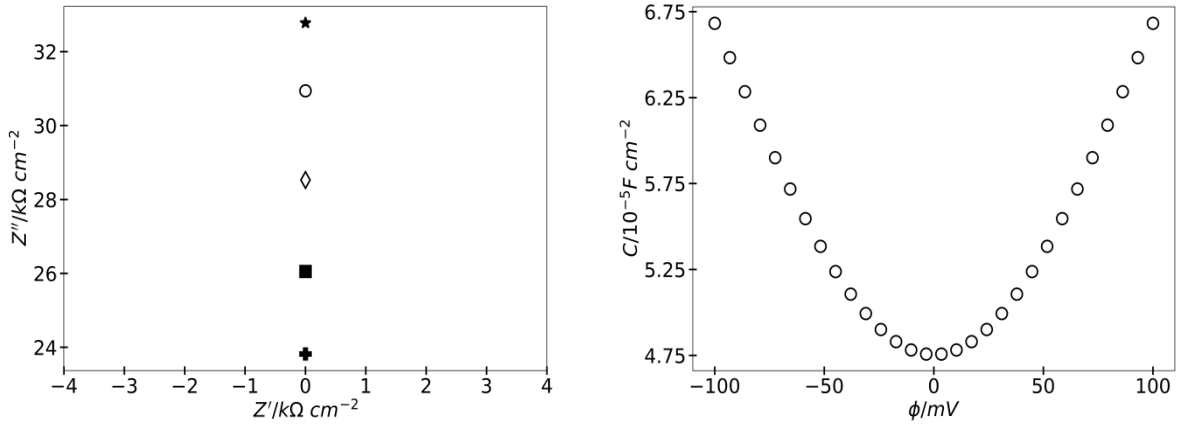

(a) Nyquist diagram for f = 1Hz **(b) Capacitance**

Fig. 8. (a) Nyquist diagram for different dc potentials and (b) capacitance as a function of applied potential from impedance study.

4. Conclusions

We presented a simple model for the study of the double layer structure. It was shown that for potentials lower than the thermal voltage ($\approx 25mV$) the linear approximation of the PNP solution is valid, while for higher potentials the complete nonlinear PNP equation is necessary for the description of the potential distribution and the space charge density. Frequency domain analysis was also carried out and the total capacitance was obtained from it. Results from impedance analysis corroborated the PNP description of the nonlinear capacitance as a hyperbolic function of potential. Therefore, our results are in agreement with the analytical predictions,

which shows that the model is suitable for the study of the structure of the EDL. Next steps include the implementation of geometrical and thermodynamic non-idealities, such as porous electrodes and concentrated solutions.

Acknowledgments

The authors would like to thank Professor Dr. Ernesto C. Pereira for making the use of COMSOL Multiphysics possible. This study was financed in part by the Coordenação de Aperfeiçoamento de Pessoal de Nível Superior - Brasil (CAPES) - Finance Code 001.

References and Notes

[1] Bockris, J. O'M.; Reddy, A. K. N.; Gamboa-Aldeco, M. Modern Electrochemistry 2A, 2nd ed. New York, Springer US, 2000.

[2] Schmickler, W.; Santos, E. Interfacial Electrochemistry, 2nd ed. New York, Springer, 2010.

[3] Tosaka/CC BY (https://creativecommons.org/licenses/by/3.0)

[4] Sharma, P.; Bhatti, T. S. *Energy Convers. Manage.* **2010**, *51*, 2901. **[Crossref]**

[5] Shao, Y.; El-Kady, M. F.; Sun, J.; Li, Y.; Zhang, Q.; Zhu, M.; Wang, H.; Dunn, B.; Kaner, R. B. *Chem. Rev.* **2018**, *118*, 9233. **[Crossref]**

[6] Conder, J.; Fic, K.; Matei Ghimbeu, C. In: Char and Carbon Materials Derived from Biomass Production, Characterization and Applications, Elsevier, 2019, 383. **[Crossref]**

[7] Monroe, C. W.; Urbakh, M.; Kornyshev, A. A. *J. Electroanal. Chem.* **2005**, *582*, 28. **[Crossref]**

[8] Koryta, J. *Electrochimica Acta* **1988**, *33*, 189. **[Crossref]**

[9] Mareček, V.; Samec, Z.; Koryta, J. *Adv. Colloid Interface Sci.* **1988**, *29*, 1. **[Crossref]**

[10] Trojánek, A.; Mareček, V.; Samec, Z. *Electrochimica Acta* **2015**, *180*, 366. **[Crossref]**

[11] Trojánek, A.; Mareček, V.; Samec, Z. *Electrochem. Commun.* **2018**, *86,* 113. **[Crossref]**

[12] Mandabattulla, G.; Gupta, S. K. COMSOL Conference – Modeling of Supercapacitors, Bangalore, Canada, 2012. **[Link]**

[13] Zhang, G. COMSOL Conference – Simulating the Electrical Double Layer Capacitance, Boston, USA, 2010. **[Link]**

[14] He, R.; Chen, S.; Yang, F.; Wu, B. *The Journal of Physical Chemistry B* **2006**, *110*, 3262. **[Crossref]**

[15] Mitropoulos, A. C. *J. Eng. Sci. Technol. Rev.* **2008**, *1*, 1. **[Crossref]**

[16] COMSOL Multiphysics® v. 5.4. www.comsol.com. COMSOL AB, Stockholm, Sweden, 2018.

[17] Reference Manual, pp. 256 and 265. COMSOL Multiphysics® v. 5.4. COMSOL AB, Stockholm, Sweden. 2018.

How to cite this article

De Moraes, A. S.; Carneiro Neto, E. B.; Lopes, M. C. *Orbital: Electron. J. Chem.* **2021**, *13*, 108. DOI: **http://dx.doi.org/10.17807/orbital.v13i2.1453**